

3. R. H. Whittaker, F. H. Bormann, G. E. Likens, T. G. Siccama, *ibid.* **44**, 233 (1974).
4. W. W. Covington, thesis, Yale University (1976).
5. C. A. Federer, *U.S. For. Res. Note NE-167* (1973).
6. G. E. Likens, F. H. Bormann, R. S. Pierce, J. S. Eaton, N. M. Johnson, *Biogeochemistry of a Forested Ecosystem* (Springer-Verlag, New York, 1977).
7. Nitrogen in aboveground and belowground living biomass pools is calculated from biomass estimated by dimensional analysis (3, 4) and nitrogen concentrations representative of vegetative components of the ecosystem (8). Organically bound nitrogen in the forest floor and mineral soil to a combined depth of 45 cm is calculated from depth, bulk density, and Kjeldahl nitrogen analyses (9). Available nitrogen content is calculated from depth, bulk density, and ammonium, nitrite, and nitrate analyses of the soil to a depth of 38 cm (10).

Values for nitrogen accretion in living biomass are calculated from annual woody biomass increments estimated by dimensional analyses (3, 4), data on woody litter (11), and Kjeldahl nitrogen analyses (8, 10, 11). Nitrogen accretion in the forest floor is estimated by using samples obtained from a successional sequence of northern hardwood stands ranging in age from 3 to about 200 years (4). Nitrogen accretion in the mineral soil is assumed to be near zero.

Since the ecosystem is a small watershed with a watertight bedrock, the only significant non-gaseous loss of nitrogen occurs as dissolved or particulate matter in water draining from the system (1). The average annual nitrogen export in stream water is based on 10 years of direct measurement (6). Gaseous loss of nitrogen resulting from denitrification is unmeasured, but is assumed to be small since the soils are acid (pH 3.9 to 4.5), well drained, and low in nitrate production (9, 10). These conditions are apparently not conducive to denitrification (12); however, incubation of KNO₃-amended soils from Hubbard Brook in a helium atmosphere for 5 weeks at 25°C suggests that these soils have a potential for denitrification (L. H. Wullstein, unpublished data).

Microbial fixation of nitrogen and nitrogen in bulk precipitation are the two major inputs considered. Microbial fixation of nitrogen is estimated by difference: annual nitrogen fixation = (annual nitrogen accretion of the system + annual hydrologic export of nitrogen) - (annual precipitation input of nitrogen). The value we report is actually an estimate of net fixation: net fixation equals fixation minus denitrification. Our estimate of net fixation is based on the average of two different periods of biomass accretion (1956 to 1960 and 1961 to 1965). If we used these as separate periods, estimated nitrogen-fixation would range from 10.9 to 17.2 kg ha⁻¹ year⁻¹. Inorganic nitrogen in bulk precipitation (wet and dry deposition) has been measured directly for 10 years and mean annual input is used (6). Based on a relatively few measurements, there apparently are negligible amounts of organic nitrogen in precipitation at Hubbard Brook.

Another possible source of nitrogen input for the ecosystem is gaseous uptake of ammonia or impaction of nitrogenous aerosols (such as ammonium sulfate) on vegetation surfaces. Preliminary evidence suggests that these inputs are small compared to the nitrogen fixed by microbial activity. Since our estimate of net microbial fixation of nitrogen for the ecosystem is obtained by difference, uptake of gaseous or impacted nitrogen would reduce the estimate for fixation.

Direct measurements of the movement of nitrogen in stemflow and throughfall (13), root exudates (14), and aboveground litter (10, 11) were made, and root litter (3, 4, 10) was estimated. Annual uptake of nitrogen by all of the plants from the soil is estimated from the sum of the nitrogen incorporated in annual woody biomass accretion and the nitrogen transferred annually from living vegetation to the soil through stemflow and throughfall, root exudates, aboveground litter, and root litter.

In the soil, transformation of organically bound nitrogen to inorganic nitrogen (available soil nitrogen) is referred to as gross N-mineralization. Only that portion of the gross not used by soil microorganisms (that is, net N-mineralization) is potentially available to the ecosystem's vascular plants. Annual net N-mineralization is estimated by difference: annual net N-mineralization = (annual nitrogen uptake by plants + annual hydrologic export of inorganic nitrogen) - (annual precipitation input of in-

organic nitrogen + annual transfer of inorganic nitrogen in stemflow and throughfall + annual transfer of inorganic nitrogen in root exudates). In estimating net N-mineralization, it is assumed that all inorganic nitrogen entering the soil as precipitation input, stemflow and throughfall, and root exudates moves directly into the available soil nitrogen pool. If this inorganic nitrogen entering the soil were first taken up by soil microorganisms and then mineralized, our net N-mineralization estimate would be larger.

At the height of the growing season, leaf tissue in this northern hardwood forest ecosystem has a nitrogen content of approximately 70 kg/ha. During senescence, the amount of nitrogen in the leaves decreases precipitously. Fresh leaf litter contains only about 30 kg/ha. Of the various pathways by which nitrogen may be removed from the leaves, it is concluded that during senescence almost 40 kg/ha is retranslocated from the leaves to the woody tissue of the hardwoods (D. F. Ryan, unpublished data). Retranslocation is estimated by difference: annual retranslocation of nitrogen = (nitrogen content of leaves prior to senescence) - (nitrogen content of leaf litter + nitrogen in throughfall and stemflow during senescence). In estimating retranslocation it is assumed that there is no aerosol impaction of nitrogen on leaf surfaces, no direct uptake of gaseous nitrogen by leaves, and no loss of gaseous nitrogen from leaves.

8. G. E. Likens and F. H. Bormann, *Yale Univ. Sch. For. Bull.* **79** (1970).
9. A. S. Dominski, thesis, Yale University (1971).
10. J. M. Melillo, thesis, Yale University (1977).
11. J. R. Gosz, G. E. Likens, F. H. Bormann, *Ecology* **53**, 769 (1972).
12. M. Alexander, *Soil Microbiology* (Wiley, New York, 1961).
13. J. S. Eaton, G. E. Likens, F. H. Bormann, *J. Ecol.* **61**, 495 (1973).
14. W. H. Smith, *Ecology* **57**, 324 (1976). Smith considers root exudate estimates as conserva-

15. P. Duvigneaud and S. Senaeyer-DeSmet, in *Analysis of Temperate Forest Ecosystems*, D. E. Reichle, Ed. (Springer-Verlag, New York, 1970), pp. 199-225.
16. G. S. Henderson and W. F. Harris, in *Forest Soils and Land Management*, B. Bernier and C. H. Winget, Eds. (Université Laval, Quebec, 1973), pp. 179-193; J. E. Mitchell, J. B. Waide, R. L. Todd, in *Mineral Cycling in Southeastern Ecosystems*, F. G. Howell, J. B. Gentry, M. H. Smith, Eds. (Energy Research and Development Administration, Washington, D.C., 1975), p. 41; R. L. Todd, J. B. Waide, B. W. Cornaby, in *ibid.*, p. 729.
17. F. H. Bormann, G. E. Likens, D. Fisher, R. S. Pierce, *Science* **159**, 882 (1968); W. H. Smith, F. H. Bormann, G. E. Likens, *Soil Sci.* **106**, 471 (1968); G. E. Likens and F. H. Bormann, in *Proceedings of the First International Congress on Ecology* (Centre for Agricultural Publications and Documentation, Wageningen, Netherlands, 1974), pp. 330-335; ———, N. M. Johnson, *Science* **163**, 1205 (1968); ———, D. W. Fisher, R. S. Pierce, *Ecol. Monogr.* **40**, 23 (1970).
18. G. L. Switzer and L. E. Nelson, *Soil Sci. Soc. Am. Proc.* **36**, 143 (1973).
19. J. P. Roskoski, thesis, Yale University (1977).
20. P. M. Vitousek and W. A. Reiners, *BioScience* **25**, 376 (1975).
21. R. S. Pierce, C. W. Martin, C. C. Reeves, G. E. Likens, F. H. Bormann, in *Symposium on Watersheds in Transition* (American Water Resources Association and Colorado State University, Fort Collins, 1972), pp. 285-295.
22. This is a contribution to the Hubbard Brook Ecosystem Study. Financial support was provided by the National Science Foundation. This work was conducted at the Hubbard Brook Experimental Forest in cooperation with the U.S. Forest Service.

16 August 1976; revised 3 December 1976

Chainlike Formation of Particle Deposits in Fluid-Particle Separation

Abstract. A theory is proposed for the formation and growth of particle dendrites on a collector placed in an aerosol or hydrosol stream. It is based on the interplay of two intrinsic properties of suspended particles: (i) their finite size and (ii) the randomness of the location of individual particles in the fluid stream. The results of simulations based on this theory resemble those obtained from experiments.

The transfer of solid particles from a flowing stream to a surface plays an important part in many physical and biological processes, such as the filtration of fluid-particle suspension, the deposition of inhaled particles, and the accumulation of particles on the walls of the arterial tree. The deposition rate depends on,

among other factors, the ratio of the particle size to the characteristic length of the collector. When this size ratio is sufficiently large, the collector surface is markedly altered as the particle deposit accumulates. The change in the surface structure, in turn, affects the rate of subsequent deposition. The dynamic aspect of the collector surface clearly has significant effects on the deposition process.

The manner in which the particle deposit forms on the collector surface is strongly influenced by two intrinsic properties of suspended particles: (i) their finite size and (ii) the randomness of the location of individual particles in the fluid stream. The purpose of this report is to explain how the interplay of these two intrinsic properties leads to the formation of chainlike particle dendrites on a collector such as a fiber in air filtration.

The structure of solid particle deposits on fibers has been observed by a number of investigators (1). Although various filtration theories have been developed

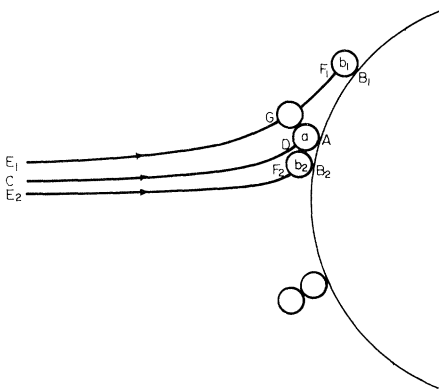


Fig. 1. Depiction of the shadowing effect and chain deposition.

since the 1930's (2), none of the existing theories makes it possible to predict in a detailed manner the process of the capture of solid particles by the collector in its entirety. In the following discussion, we assume that the particle trajectory depends only on the particle inertia and the drag force. This explanation can be readily extended to other cases where gravitational, electrostatic, and magnetic forces are present.

The finiteness of the particle size gives rise to two closely related phenomena, (i) a shadowing effect and (ii) chain deposition, which are described below.

The upper part of Fig. 1 depicts the cross section of a fiber and three particle trajectories, which are obtained by solving the equations of motion. Particle *a* which arrives at point C from upstream continues to follow trajectory CD until it deposits on the fiber at point A. Once it has deposited, particle *a* creates a shadow area, represented by arc B_1B_2 , within which no particle can deposit. Point B_1 is the point of contact between the fiber and particle b_1 , which follows trajectory E_1F_1 and just moves past particle *a* when it is at point G. Similarly, point B_2 is the point of contact between the fiber and particle b_2 , which just escapes capture by particle *a* and deposits on the fiber in its immediate neighborhood. The inhibition of further deposition within the shadow is clearly an important factor which leads to non-uniform deposition.

Table 1. Sequence of particle deposition in a simulation, with resulting changes in dendrite distribution and collection efficiency.

Particle number	Initial position	Type of collection	Dendrite size distribution	Collection efficiency
Clean fiber				
1	17	P	(1)	0.26
2	54	N	(1)	0.56
3	67	N	(1)	0.56
4	37	S	(2)	0.79
5	04	P	(2,1)	0.79
6	92	N	(2,1)	0.79
7	05	S	(2,2)	0.79
8	24	S	(3,2)	0.79
9	62	N	(3,2)	0.79
10	15	S	(3,3)	0.79
11	55	S	(4,3)	1.05
12	12	S	(4,4)	1.05
13	12	S	(4,5)	1.05
14	92	N	(4,5)	1.05
15	81	N	(4,5)	1.05
16	59	S	(5,5)	1.07
17	07	S	(5,6)	1.07

A deposited particle protrudes above the fiber surface and hence provides a new surface area greater than the area of the fiber it occupies. As a result, the particle has a greater chance to capture oncoming particles than an equivalent fiber surface (equal to the projected area of the particle) does. When a second particle is captured by the first particle, a chainlike two-particle dendrite is formed, such as that shown in the lower part of Fig. 1. The

new dendrite has an even greater surface area and hence greater capture efficiency. Thus, the deposition of the first particle at a given site touches off a chain reaction there.

The number of dendrites formed on a given length of the fiber and the size and shape of these dendrites are determined by the location of individual particles arriving from upstream and the order of their arrival. Although the concentration distribution of suspended particles in the stream far away from the surface can be considered as uniform, the location of individual particles is intrinsically stochastic in nature. This aspect is particularly important in situations where the number of particles involved is relatively small, such as in the formation and growth of a particle dendrite. By taking into account the randomness of individual particles together with their trajectories determined from the equations of motion, we can construct a graph depicting the formation and growth of dendrites on the collector. This process is illustrated in Fig. 2, which depicts a quarter of the cross section of a fiber with a family of trajectories.

To construct a graph showing the formation and growth of dendrites, we first find the location y_0 of individual particles arriving at $x = -2d_f$. Consider a height $5d_p$, which is divided into 100 equal intervals, numbered consecutively from 0 to 99 (Fig. 2). (The choices of the height and the number of intervals will be discussed later.) Since the particle concentration in the approaching stream can be considered as uniform at $x = -2d_f$, each of these 100 intervals has an equal chance to receive the oncoming particles. However, because the order of arrival among these intervals is stochastic in nature, a sequence of y_0 's representing the location and order of arrival of individual particles at $x = -2d_f$ can be determined by a set of random numbers in the range of 0 to 99. Column 2 in Table 1 gives a set of such numbers, and the dendrites formed by this sequence of arrivals are shown in Fig. 2. Particle 1, starting from position 17 and following its trajectory, deposits at point A. Particles 2 and 3, starting from positions 54 and 67, respectively, are too far from the surface to be collected. Particle 4, starting from position 37, deposits on particle 1, thereby forming a two-particle dendrite. It can be seen at this stage that, depending on its initial location, a particle can deposit on the fiber (primary deposition), can collide with a particle dendrite (secondary deposition), or can continue past the collector. These possibilities are indicated by P, S, and N, respectively, in column 3 of Table 1. The construction of a graph such as

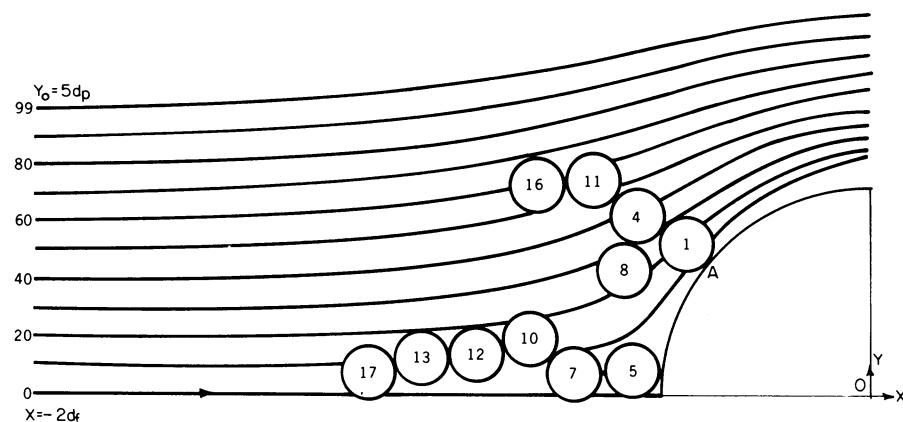


Fig. 2. Formation and growth of particle dendrites on a fiber. One obtains the particle trajectories by solving the equations of motion of a particle with a potential flow field around the fiber. The trajectories are almost parallel at $x = -2d_f$. Values of the physical parameters used are as follows: d_p (particle diameter) = $1.305 \mu\text{m}$; d_f (fiber diameter) = $9.6 \mu\text{m}$; U (air velocity in the main stream) = 13.8 cm/sec ; ρ (particle density) = 1 g/cm^3 ; the corresponding Stokes number is $(\rho d_p^2 U / 9 \mu d_f) = 0.15$, where μ is the viscosity of air.

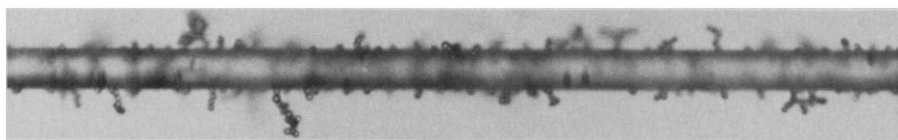


Fig. 3. Dendrites of $1.305\text{-}\mu\text{m}$ polystyrene latex spheres formed on a single glass fiber $8.7 \mu\text{m}$ in diameter at an air velocity of 13.8 cm/sec (3).

that shown in Fig. 2 can be considered as a simulation. The simulation under consideration involves only 17 particles. Two dendrites are formed, the upper one having five particles and the lower one having six particles. Column 4 in Table 1 gives the matrix which represents the size of the two dendrites in the order of their formation. The distribution of dendrites is asymmetrical over the fiber. For an accurate simulation the entire front surface of the fiber should be considered.

One of the important parameters in filtration theory is the collection efficiency of single fibers, defined as the ratio $2y_{oc}/d_f$, where y_{oc} is the initial y coordinate of the particle which just moves past the collector. The trajectory of such a particle, called the limiting trajectory, moves farther away from the collector surface whenever a newly deposited particle protrudes in the cross-stream direction beyond the old surfaces. This can be seen in Fig. 2. The clean fiber has a y_{oc} of $0.13 d_f$. After the first particle deposits, y_{oc} increases to $0.28 d_f$. The change in collection efficiency is shown in column 5 of Table 1 for the simulation under consideration.

Repeated simulations with different sets of random numbers would generate an ensemble of dendrites resembling those actually formed on a piece of fiber shown in Fig. 3. The number of particles used in each simulation is determined by the particle concentration, the filtration time, and the height used in the simulation. The only requirement in selecting the height is that it should be greater than the final value of y_{oc} when the simulation is stopped. For simplicity, the simulation

is carried out on a single cross section. A more realistic construction can be made by taking into account the randomness of the location of individual particles along the fiber length.

The above discussion explains how the interplay of the finite size of particles and the stochastic nature of the location of individual particles leads to the formation and growth of chainlike particle deposits. Other important parameters such as the Stokes number and the ratio of the particle size to the collector diameter would also influence the shape of the dendrites. Long dendrites tend to form near the front of the cylinder at high Stokes numbers, whereas they tend to form near the sides at low Stokes numbers. Conceivably, the deposit would become increasingly smoother as the size ratio decreases. An artifact of the simulation is that the shape of dendrites also depends on the size of the intervals Δy_0 used. In the simulation discussed above, Δy_0 is equal to $0.05 d_p$. The form of the dendrites would become more realistic as the size of intervals is further reduced.

CHI TIEN

CHIU-SEN WANG, D. T. BAROT

*Department of Chemical Engineering
and Materials Science, Syracuse
University, Syracuse, New York 13210*

References and Notes

1. C. E. Billings, thesis, California Institute of Technology (1966). This thesis includes a thorough review of earlier studies.
2. See the review by C. N. Davies [*Air Filtration* (Academic Press, New York, 1973)] and the new theory proposed by A. C. Payatakes and C. Tien [*J. Aerosol Sci.* 7, 85 (1976)].
3. The photograph in Fig. 3 was taken by C. E. Billings. We thank him for providing the negative.

23 August 1976; revised 23 November 1976

Pyroelectricity and Induced Pyroelectric Polarization in Leaves of the Palmlike Plant *Encephalartos villosus*

Abstract. *Quantitative pyroelectric measurements were made on the leaves of the palmlike plant Encephalartos. A pyroelectric response almost 50 times higher than the normal one could be induced by a small bias electric field, offering a means for highly increasing the efficiency of conversion of thermal to electrical energy. No evidence of ferroelectricity was found.*

Qualitative observations of the pyroelectric effect in the epidermis of the leaves of the palmlike gymnosperm plant *Encephalartos villosus* (family Cycadaceae) were first made by Athenstaedt (1). He observed that the orientation of the pyroelectric vector was such that the outer surfaces of the leaves became positive on heating. In the research we report here, the earlier observations were confirmed, proof was found that the effects observed are thermally in-

duced and not photoinduced, and quantitative values were measured. Most important, we found that a pyroelectric polarization almost 50 times higher than the normal response could be induced by a small bias electric field. This effect, to our knowledge not previously observed in any other materials, offers a highly increased efficiency of conversion of thermal to electrical energy. No evidence of ferroelectricity was observed in the material.

The pyroelectric effect was measured by exposing thin samples of material to short rectangular pulses of light from a xenon lamp. The electric charges released were measured by a charge amplifier, the output of which was displayed on an oscilloscope. The intensity of the illumination was determined by calibration with tourmaline, and voltage-time curves were analyzed according to the method of Simhony and Shaulov (2). A sample was prepared from a fresh leaf by scraping away material from one surface with a scalpel until the thickness of the other epidermis was in the range 0.06 to 0.12 mm. A piece about 0.5 to 1.0 cm² in cross-sectional area was cut out. The sample was air-dried for 5 to 10 minutes and then attached to a copper electrode with silver paste. The free surface was also coated with silver paste, and electrical contact was made by means of a copper spring. The electrical resistance of the materials was of the order of 10¹¹ ohms after preparation and did not change significantly over several days, indicating that the samples were dry at all times. Temperature variation of the sample from -20° to 45°C was possible.

To demonstrate that the electrical response to the light pulses was truly a pyroelectric effect and not a photoeffect, the light was partially absorbed by a series of optical filters. Measurements were made with the epidermis samples as well as with a copper-constantan thermocouple, tourmaline, and bovine tendon. The pyroelectric properties of tourmaline have been known since antiquity (3), and tendon was previously shown to be pyroelectric by Lang (4), using a heating and cooling technique. All of the materials examined were painted with the same silver paste. Figure 1 shows the electrical response (relative to that with unfiltered light) for each material plotted against the 50 percent transmission points of the filters. For comparison with a typical photosensitive material, a similar curve for a silicon photodiode was recorded. The response of the epidermis is clearly due to a change in temperature, and thus the effect is a pyroelectric one.

The measurement method used gives the ratio of the pyroelectric coefficient to the product of the density and the heat capacity, $p/\rho c$ (in coulomb cm joule⁻¹). Precise values of the density and the heat capacity have not yet been determined, but estimates of 0.9 g cm⁻³ and 1.4 joule g⁻¹ °C⁻¹, respectively, are used here. The pyroelectric coefficient of the epidermis of *Encephalartos* showed typical biological scatter, having a value (mean \pm standard deviation) of $1.3 \pm 0.4 \times$